thermo scientific

Lead discovery

When you need to be at the forefront of discovery, the very highest data quality and comprehensive quantitative information are paramount. Advance your science and adapt to evolving research demands with the unprecedented performance and versatility of the Thermo Scientific™ Orbitrap Exploris™ GC 240 mass spectrometer. Get the right answer the first time and solve complex analytical challenges with easy access to the very highest-accuracy, information-rich GC-MS data, today and well into the future.

Delivering broader and deeper insights

Find out more at **thermofisher.com/OrbitrapExplorisGC240**

ThermoFisher SCIENTIFIC

Received: 3 October 2020 | Revised: 27 October 2020 | Accepted: 30 October 2020

DOI: 10.1002/rcm.8998

RESEARCH ARTICLE

Rapid Communications in Mass Spectrometry WILEY

Formation of positive product ions from substances with low proton affinity in high kinetic energy ion mobility spectrometry

Maria Allers | Ansgar T. Kirk | Christoph Schaefer | Florian Schlottmann | Stefan Zimmermann

Leibniz University Hannover, Institute of Electrical Engineering and Measurement Technology, Hannover, Germany

Correspondence
M. Allers, Institute of Electrical Engineering and Measurement Technology, Leibniz University Hannover, Appelstraße 9a, 30167 Hannover, Germany.
Email: allers@geml.uni-hannover.de

Funding information
Deutsche Forschungsgemeinschaft, Grant/Award Numbers: BE 2124/8-1, ZI 1288/8-1

Rationale: Ion mobility spectrometry (IMS) instruments are typically equipped with atmospheric pressure chemical ionization (APCI) sources operated at ambient pressure. However, classical APCI-IMS suffers from a limited ionization yield for nonpolar substances with low proton affinity (PA). This is mainly due to ion clustering processes, especially those that involve water molecules, inhibiting the ionization of these substances.

Methods: High Kinetic Energy (HiKE)-IMS instruments are operated at decreased pressures and high reduced electric field strengths. As most clustering reactions are inhibited under these conditions, the ionization yield for nonpolar substances with low PA in HiKE-IMS should differ from that in classical APCI-IMS. To gain first insights into the ionization capabilities and limitations of HiKE-IMS, we investigated the ionization of four model substances with low PA in HiKE-IMS using HiKE-IMS-MS as a function of the reduced electric field strength.

Results: The four model substances all have proton affinities between those of H_2O and $(H_2O)_2$ but exhibit different ionization energies, dipole moments, and polarizabilities. As expected, the results show that the ionization yield for these substances differs considerably at low reduced electric field strengths due to ion cluster formation. In contrast, at high reduced electric field strengths, all substances can be ionized via charge and/or proton transfer in HiKE-IMS.

Conclusions: Considering the detection of polar substances with high PAs, classical ambient pressure IMS should reach better detection limits than HiKE-IMS. However, considering the detection of nonpolar substances with low PA that are not detected, or only difficult to detect, at ambient pressure, HiKE-IMS would be beneficial.

1 | INTRODUCTION

Due to their high sensitivity, fast response times, and compact design, ion mobility spectrometers are commonly used in safety and security applications such as the detection of chemical warfare agents,[1,2] toxic industrial chemicals,[3,4] drugs,[5,6] and explosives.[7–9] Basically, ion mobility spectrometry (IMS) instruments can be divided by their principle of ion separation. In this work, a drift tube (DT) ion mobility spectrometer is used. In DT-IMS, ions are separated by their motion along the axis of a drift tube driven by a homogeneous static electric field. To initiate the measurement, an ion packet is injected into the drift tube. During their motion, the ions are separated based on the absolute value of their ion mobility in the present drift gas. At the end of the drift tube, the ions are captured by a detector that converts

and amplifies the ion current into a measurable voltage. By plotting the measured voltage over the drift time, that is, the time that the ions need to reach the detector, an ion mobility spectrum is obtained. Typically, ion mobility spectrometers are equipped with atmospheric pressure chemical ionization (APCI) sources operated at ambient pressure. Here, the ionization proceeds in two steps. Initially, stable reactant ions are generated by ionizing the main constituents of the sample gas. In a second step, ionization of analyte molecules follows through reactions with these reactant ions. Due to the large number of collisions at ambient pressure, IMS with APCI sources can achieve limits of detection in the low ppt_v (parts-per-trillion by volume) range in measurement times of less than a second for a broad range of substances.[10,11]

Although this renders APCI-IMS at ambient pressure a very sensitive and versatile detection method with considerably low instrumental effort, it suffers from a low linear range, strong matrix effects, and a limited ionization yield for a number of compound classes. The ionization yield strongly depends on the generated reactant ion species. Typically, the positive reactant ions $H_3O^+(H_2O)_n$ and the negative reactant ions $O_2^-(H_2O)_n$ are formed in purified air at ambient pressure through reverse-flow continuous corona discharge ionization sources.[12–15] Their cluster size n depends on the background water concentration and the reduced electric field strength E/N, where E/N is the ratio of the electric field strength E to the neutral molecule density N, usually expressed in Townsend (1 Td = 1×10^{-21} Vm^2). In this context, the reduced field is a measure of the average ion kinetic energy resulting from acceleration in the electric field and deceleration by collisions with neutrals. On increasing the background water concentration, the cluster size increases, whereas on increasing the reduced electric field strength E/N, the cluster size decreases due to collision-induced cluster dissociation reactions. In the positive ion mode, the hydrated hydronium ions $H_3O^+(H_2O)_n$ can ionize analyte molecules via proton transfer or ligand-switching reactions.[10,16] Proton transfer reactions (PTRs) are possible when the proton affinity (PA) of the analyte molecule exceeds that of $(H_2O)_{n+1}$, whereas the efficiency of the ligand-switching reactions seems to depend on the dipole moment and the polarizability of the analyte molecule.[10,17,18] In the negative ion mode, the oxygen-based water clusters $O_2^-(H_2O)_n$ can ionize the analyte molecules via charge transfer reactions. These charge transfer reactions are effective when the electron affinity of the analyte molecule exceeds that of $O_2(H_2O)_n$. Furthermore, $O_2^-(H_2O)_n$ might react with analyte molecules via proton abstraction if the gas-phase acidity of the analyte molecule exceeds that of $HO_2(H_2O)_n$. Thus, in APCI-IMS operated at ambient pressure, polar substances with high PA or high electron affinity are detected with the highest sensitivity. In contrast, nonpolar substances with low PA or low electron affinity are difficult to detect or are not detected at all.

To overcome these limitations, we introduced High Kinetic Energy IMS (HiKE-IMS).[19,20] As in the classical DT-IMS method operated at ambient pressure, in HiKE-IMS, ions are generated in a reaction region by a reverse-flow continuous corona discharge ionization source before ions are separated in a drift region. In contrast to classical IMS, HiKE-IMS instruments are operated at a decreased pressure between 10 and 40 mbar to reach high reduced electric field strengths in both the reaction region and the drift region. As known from PTR-MS,[16] operation at decreased pressure and high reduced electric field strengths might be beneficial for two main reasons: First, the much-shorter and better-defined residence time of ions in the reaction region might lead to an increase in the linear range and a decrease in chemical cross-sensitivities. Second, at elevated reduced electric field strengths, all charge-bound cluster formation equilibria are shifted toward smaller sizes, enabling other ionization pathways to ionize even substances with low PA or low electron affinity not detectable by APCI.

However, until now, only limited knowledge about the ionization processes occurring in HiKE-IMS has been available. In previous studies, the prevailing reactant ion population in HiKE-IMS has been identified by coupling a HiKE-IMS instrument to a mass spectrometer.[21–23] Due to operation at decreased pressure and high reduced electric field strengths, the reactant ion population in HiKE-IMS can significantly differ from that in classical ambient pressure IMS. For example, in positive ion mode, in addition to $H_3O^+(H_2O)_n$, considerable levels of $O_2^+(H_2O)_n$ and $NO^+(H_2O)_n$ ions may occur in HiKE-IMS depending on the operational parameters. Furthermore, in negative ion mode, $O^-(H_2O)_n$, $O_3^-(H_2O)_n$, and $CO_3^-(H_2O)_n$ ions have been observed in addition to $O_2^-(H_2O)_n$. The presence of these ions indicates that the mechanisms underlying the ionization of analyte molecules in HiKE-IMS might be rather complex. Nonetheless, the presence of these ions enables new ionization pathways to ionize substances not accessible by APCI. Thus, a profound knowledge of the ionization mechanisms in HiKE-IMS is essential to estimate its capabilities and limitations regarding the detection of analyte molecules.

The aim of this work is to gain first insights into the ionization processes in HiKE-IMS leading to the formation of positive product ions from substances with low PA. The mechanisms underlying the formation of negative product ions will be investigated in a separate paper, as a description of all ionization processes would exceed the scope of this paper. In this work, first, a theoretical overview of the possible ionization pathways resulting in positive product ions in APCI sources is given. Subsequently, the HiKE-IMS ionization of the four exemplary model substances, acetonitrile, methanol, phosphine, and benzene, is investigated as a function of the reduced electric field strength and the humidity in the reaction region. The occurring product ion species are identified using HiKE-IMS-MS.[21]

2 | EXPERIMENTAL

2.1 | HiKE-IMS

A detailed description of the HiKE-IMS setup was previously provided by Kirk et al.[24] The operating parameters used in this work are presented in Table 1. To identify individual ion species associated

TABLE 1 HiKE-IMS operating parameters

Parameter	Value
Temperature	45°C
Operating pressure	14.3 mbar
Drift gas	Purified air containing 50 ppm_v H_2O
Drift gas flow	19 mL_s/min[a]
Sample gas	Purified air containing 50–4000 ppm_v H_2O
Sample gas flow	19 mL_s/min[a]
Drift region length	306 mm
Reduced electric field strength in the drift region	110 Td
Reaction region length	77 mm
Reduced electric field strength in the reaction region	Up to 115 Td
Injection time	1 µs
Ionization source	CD
CD voltage	1250 V
CD current	3 µA
Effective CD voltage	930 V

CD, corona discharge; HiKE-IMS, High Kinetic Energy Ion Mobility Spectrometry.
[a]mL_s/min: milliliter standard per minute; mass flow at reference conditions 20°C and 1013.25 hPa.

with signals in the ion mobility spectrum, the HiKE-IMS-MS coupling described in a previous work[21] is used. It should be noted that the HiKE-IMS instrument may generally be operated at pressures between 10 and 40 mbar. However, in this work, the operating pressure is constant at 14.3 mbar, as the HiKE-IMS-MS coupling requires a pressure of ~14 mbar.

2.2 | Gas supply

Purified air containing <1 ppm_v of water was supplied by a zero-air generator (JAGZAG600S, JA-Gas Technology, Burgwedel, Germany) combined with a CAS1 pressure swing absorber (Pure Gas Products, Frechen, Germany) in series with an additional moisture trap (Supelco, molecular sieve 5A moisture trap, 23991, Merck, Darmstadt, Germany) and an activated carbon filter (Supelcarb HC hydrocarbon trap, 24564, Merck). The water concentration in the sample gas and in the drift gas can be independently adjusted by mixing the supplied purified air with air that is passed through a water container. The resulting sample gas humidity and the drift gas humidity are measured by dew point sensors (Easidew Transmitter, Michell Instruments, Friedrichsdorf, Germany). Due to diffusion through seals and tubings, the residual water concentration in the HiKE-IMS instrument may well exceed 1 ppm_v. To prevent the water concentration in the instrument from being affected by this diffusion, the lowest water concentration in the sample and drift gas was intentionally increased to 50 ppm_v.

3 | IONIZATION PATHWAYS RESULTING IN THE FORMATION OF POSITIVE PRODUCT IONS IN HIKE-IMS

In previous studies, the prevailing positive reactant ion population in HiKE-IMS was identified by coupling the HiKE-IMS instrument to a mass spectrometer,[21] and $H_3O^+(H_2O)_n$, $NO^+(H_2O)_n$, and $O_2^+(H_2O)_n$ ions were observed. At thermal ion–molecule interaction energies, extensive information is available from selected ion flow tube mass spectrometry studies concerning the reactions of H_3O^+, NO^+, and O_2^+ with various analyte molecules.[25–39] Furthermore, PTR-MS[40,41] and selective reagent ionization time-of-flight-MS[42,43] studies deliver information at elevated ion–molecule interaction energies. According to these studies, various ionization pathways are possible in HiKE-IMS, ranging from simple charge transfer to chemical reactions such as proton transfer or ligand switching, which may result in the formation of multiple product ion species per analyte molecule species. However, the abundances of the $H_3O^+(H_2O)_n$, $NO^+(H_2O)_n$, and $O_2^+(H_2O)_n$ reactant ions in HiKE-IMS significantly depend on the reduced electric field strength, the water concentration of the reaction region, and the pressure (here constant at 14.3 mbar).[22] Furthermore, it should always be kept in mind that the additional collision energy caused by the high reduced electric field strengths in HiKE-IMS can enhance the degree of fragmentation.

Here, the relevant ionization pathways initiated by each reactant ion species are considered in detail. To predict whether a reaction occurs, thermodynamic data are included. The crucial variable required to evaluate the spontaneity of a chemical reaction is the change in the Gibbs energy, ΔG, where G represents the Gibbs energy and Δ refers to the difference in values between products and reactants. A chemical reaction is thermodynamically spontaneous if the Gibbs energy change for the reaction is negative.[44] However, it is noteworthy that a spontaneous process may proceed quickly or slowly, as spontaneity is not related to kinetics or reaction rate. According to Equation 1, the change in the Gibbs energy ΔG_T^0 at constant temperature T can be calculated from the change in the enthalpy ΔH_T^0 and the change in the entropy ΔS_T^0:

$$\Delta G_T^0 = \Delta H_T^0 - T\Delta S_T^0, \quad (1)$$

where T is the absolute temperature and the superscript 0 refers to the standard state. In the ionization reactions considered in this work, the entropy change ΔS_T^0 is typically negligibly small, as a proton or a charge is a simple entity whose transfer from one molecule to another does not significantly alter the net system entropy. Thus, in almost all practical cases, an ionization reaction occurs spontaneously if the change in the reaction enthalpy ΔH is negative.[16]

1. Reactions of hydrated hydronium cations $H_3O^+(H_2O)_n$

Typically, the hydronium cation H_3O^+ reacts with analyte molecules M via exothermic proton transfer, as illustrated by reaction 2.[45] The

reaction rate constant for such a reaction is usually of the order of magnitude of the collision rate constant:[46]

$$H_3O^+ + M \rightarrow MH^+ + H_2O \quad \text{if } PA(M) > PA(H_2O). \tag{2}$$

If the PA of the analyte molecule exceeds that of H_2O (691 kJ/mol[47]), the proton transfer reaction (2) occurs spontaneously.

However, in the presence of water, H_3O^+ ions form stable water clusters via the three-body cluster association reaction 3. For example, hydrated hydronium cations $H_3O^+(H_2O)_n$ with a cluster size of $n = 3$ are expected to be major species in a thermally equilibrated system at ambient pressure and <1 ppm_v humidity:[48]

$$H_3O^+(H_2O)_{n-1} + H_2O + A \rightleftharpoons H_3O^+(H_2O)_n + A. \tag{3}$$

According to previous studies,[49–51] water clusters $(H_2O)_{n+1}$ have higher PAs than the bare water molecule H_2O. The higher PA is the result of the added stability of H_3O^+ brought about by sharing the positive charge with additional water molecules.[16] Thus, the formation of water clusters may inhibit ionization via PTRs.

Nonetheless, ionization of analyte molecules by hydrated hydronium ions $H_3O^+(H_2O)_n$ may proceed via ligand-switching reactions. In these reactions, a water molecule is displaced by the analyte molecule M as illustrated in reaction 4:[18]

$$H_3O^+(H_2O)_n + M \rightarrow MH^+(H_2O)_{n-m+1} + m \cdot H_2O. \tag{4}$$

These ligand-switching reactions may occur if the switching process is sufficiently exothermic.[18] This may be achieved when the hydration energy of the analyte molecules is comparable with that of H_2O. Thus, the permanent dipole moment and the polarizability of the analyte molecule seem to be key parameters to predict whether ligand-switching reactions occur.[10,17,18,52]

However, as shown in several studies,[17,18,52–54] the rate constants of the ligand-switching reactions typically decrease with increasing water cluster size *n*. Therefore, increasing the sample gas humidity and thus the humidity in the reaction region results in a decrease in the sensitivity. In particular, IMS instruments operated at ambient pressure thus suffer from a sample gas humidity-dependent detection of analytes.[10,55]

To minimize the influence of the sample gas humidity on the sensitivity, the HiKE-IMS instrument is operated at high reduced electric field strengths. In this context, the reduced field is a measure of the average ion kinetic energy. On increasing the reduced electric field strength, collision-induced dissociation of water clusters occurs. For example, $H_3O^+(H_2O)$ dissociates between 90 and 110 Td, dependent on the background water concentration and the operating pressure.[41,56] However, particularly when investigating very humid samples or when operating at low reduced electric field strengths, hydrated ions still exist in the HiKE-IMS instrument. Therefore, it is important to be aware of the impact that humidity has on the ionization of analyte molecules.

2. Reactions of hydrated nitrosonium cations $NO^+(H_2O)_n$ and oxygen cations $O_2^+(H_2O)_n$

Several modes of reaction between NO^+ or O_2^+ and analyte molecules are possible. As is known from PTRs, almost all reactions proceed at or close to their respective collisional rates. The key quantities in determining the spontaneity of the reaction are the first ionization energies (IEs) of NO (9.26 eV[47]) and O_2 (12.07 eV[47]).

Analyte molecules M with IEs below these values may undergo rapid charge-transfer reactions with NO^+ and O_2^+, as shown in reactions 5 and 6, respectively:[28,33]

$$NO^+ + M \rightarrow M^+ + NO \quad \text{if } IE(M) < IE(NO), \tag{5}$$

$$O_2^+ + M \rightarrow M^+ + O_2 \quad \text{if } IE(M) < IE(O_2). \tag{6}$$

However, due to the higher IE of O_2, there is a high amount of excess energy from charge transfer with O_2^+ that will be deposited in the product ion and may result in its fragmentation.[45]

For the sake of completeness, it should be mentioned that ion–molecule association reactions that include a third body A (reaction 7) have also been reported for NO^+ if the IE of the analyte molecule is similar to that of NO.[25,31] However, it is to be expected that these association channels will be inhibited at elevated reduced electric field strengths in HiKE-IMS:

$$NO^+ + M + A \rightleftharpoons NO^+.M + A. \tag{7}$$

Similar to H_3O^+, NO^+ and O_2^+ form clusters with water molecules. However, it is noteworthy that $NO^+(H_2O)_n$ and $O_2^+(H_2O)_n$ are stable only up to a critical cluster size. If this critical size is surpassed, the ions are converted into $H_3O^+(H_2O)_n$. Thus, the abundances of $NO^+(H_2O)_n$ and $O_2^+(H_2O)_n$ ions in the HiKE-IMS experiment change with the sample gas humidity and thus the reaction region humidity.[22]

So far, there have been very few studies on the reactions of $NO^+(H_2O)_n$ and $O_2^+(H_2O)_n$ with analyte molecules. As stated in the study of Smith et al,[57] the IE of $NO(H_2O)$ (8.54 eV) is lower than that of NO (9.26 eV). Thus, the formation of $NO^+(H_2O)_n$ and $O_2^+(H_2O)_n$ clusters may inhibit ionization via charge-transfer reactions. Nonetheless, similar to $H_3O^+(H_2O)_n$, the ionization of analyte molecules by $NO^+(H_2O)_n$ may proceed via ligand-switching reactions.

4 | RESULTS AND DISCUSSION

The ionization pathways occurring in HiKE-IMS significantly depend on the reduced electric field strength in the reaction region, affecting both the ion's residence time in the reaction region and its kinetic energy. Thus, in the presented measurements, the dependence of the product ion population on this parameter is investigated.

4.1 | Positive reactant ion population inside the reaction region

As the ionization pathways in HiKE-IMS are determined by the prevailing reactant ion population, the reactant ion spectrum is considered first. Figure 1A shows the recorded reactant ion spectra for different reduced electric field strengths in the reaction region at a constant reduced electric field strength of 110 Td in the drift region. In these measurements, the water concentration in the drift gas is kept constant at 50 ppm_v, whereas the sample gas contains a constant water concentration of 4000 ppm_v (thus, the overall water concentration in the reaction region is ~2000 ppm_v due to mixing the same amounts of sample and drift gas in the reaction region). The comparably high sample gas humidity has been chosen to simulate the operation of HiKE-IMS in field applications with a direct sample gas inlet, where the sample gas humidity is typically 4000 ppm_v (corresponding to 20% relative humidity at 25°C) or higher. In the spectrum, three distinct peaks occur. In previous works, the ion species underlying these peaks have been identified as $NO^+(H_2O)_n$, $H_3O^+(H_2O)_n$, and $O_2^+(H_2O)_n$.[21,22] Increasing the reduced electric field strength in the reaction region, the total charge in the spectrum increases due to reduced Coulomb repulsion.[58] However, when investigating chemical reactions leading to the conversion of ion species, it is more useful to consider relative abundances instead of absolute abundances. The relative abundance of a certain ion species is calculated from the absolute charge underlying the respective peak of the ion species divided by the charge underlying the total ion mobility spectrum. In the following text, only relative abundances of ion species are considered. As shown in Figure 1B, on varying the reduced electric field strength in the reaction region, the relative abundances of $NO^+(H_2O)_n$, $H_3O^+(H_2O)_n$, and $O_2^+(H_2O)_n$ change. At the lowest-reduced electric field strength in the reaction region of 20 Td, only $H_3O^+(H_2O)_n$ ions are observed in the ion mobility spectrum. On increasing the reduced electric field strength in the reaction region above 40 Td, $NO^+(H_2O)_n$ ions occur in the spectrum, and on increasing the reduced electric field strength even further to above 100 Td, small amounts of $O_2^+(H_2O)_n$ ions are observed.

When interpreting the HiKE-IMS spectra presented in Figure 1, it is important to note that the reduced electric field strength in the drift region was set to a high value of 110 Td. Furthermore, the water concentration in the drift gas was kept constant at a low value of 50 ppm_v. Under these conditions, conversion reactions inside the drift region are inhibited, as well as cluster association or dissociation reactions.[22] Thus, the HiKE-IMS spectra shown in Figure 1 represent the relative abundances of $NO^+(H_2O)_n$, $H_3O^+(H_2O)_n$, and $O_2^+(H_2O)_n$ at the end of the reaction region. However, when evaluating the ionization pathways in HiKE-IMS, the reactant ion population *inside* the reaction region is relevant. As known from previous studies,[21,22] field- and moisture-dependent conversion reactions of $O_2^+(H_2O)_n$ and $NO^+(H_2O)_n$ into protonated water clusters $H_3O^+(H_2O)_n$ proceed in the reaction region of the HiKE-IMS instrument. Thus, the reactant ion population inside the reaction region significantly differs from the population at the end of the reaction region, shown in Figure 1. To illustrate this deviation, the ion–molecule reactions inside the reaction region were simulated using a simple kinetic model in MATLAB (MathWorks, Natick, MA, USA) whose parameters are described in detail in a previous work.[22] This kinetic model includes bimolecular charge-transfer reactions, cluster association and cluster dissociation reactions, and their corresponding reaction rate constants known from the literature. Using van't Hoff equations,[44] the field dependence of cluster dissociation rate constants is estimated from the rate constant of the cluster association reaction, its molar standard reaction enthalpy, its molar standard reaction entropy, and the field-dependent effective ion temperature according to Wannier.[59] Assuming a temperature of 45°C, a pressure of 14.3 mbar, and a background water concentration of 2000 ppm_v (resulting from mixing sample gas containing 4000 ppm_v of water with the same amount of drift gas containing 50 ppm_v of water in the reaction region), the kinetic model delivers the relative abundances of $NO^+(H_2O)_n$, $H_3O^+(H_2O)_n$, and $O_2^+(H_2O)_n$ depending on the position in the reaction region (see Figure 2).

At the reduced electric field strength in the reaction region of 35 Td, only $H_3O^+(H_2O)_n$ ions are experimentally observed in the HiKE-IMS spectrum, because $NO^+(H_2O)_n$ and $O_2^+(H_2O)_n$ ions are

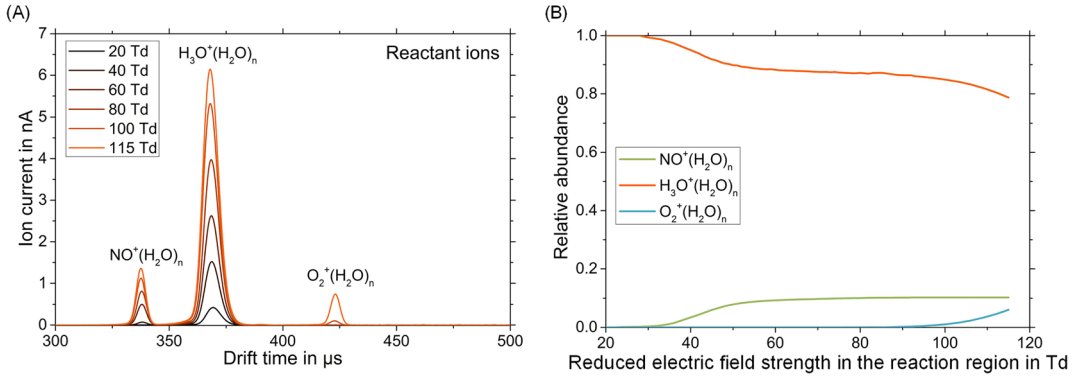

FIGURE 1 A, Measured HiKE-IMS spectra of positive reactant ions at different reduced electric field strengths in the reaction region; B, measured relative abundances of the ion species forming the ion mobility spectra depending on the reduced electric field strength in the reaction region. The sample gas humidity is 4000 ppm_v. The other operating parameters are provided in Table 1

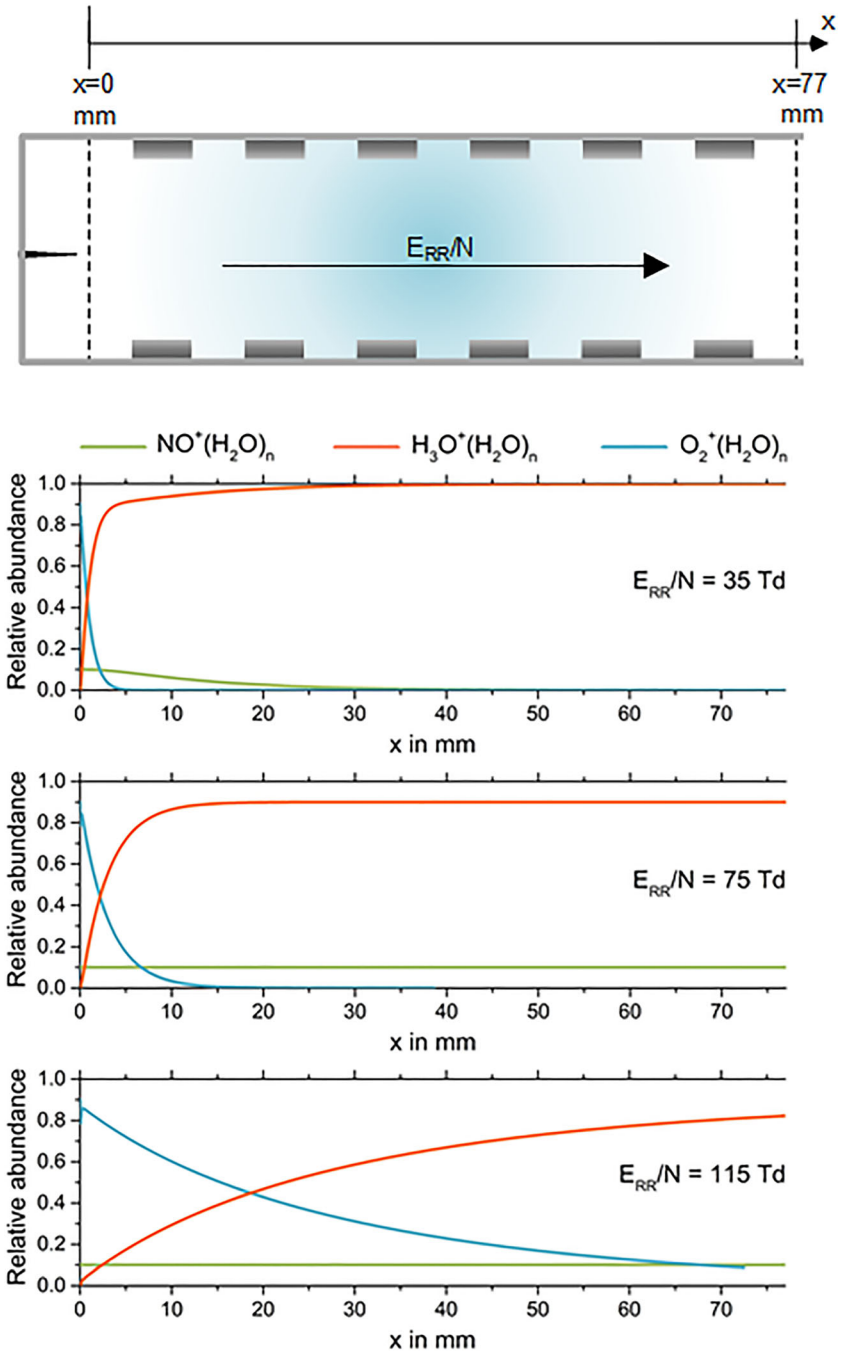

FIGURE 2 Simulated relative abundances of $NO^+(H_2O)_n$, $H_3O^+(H_2O)_n$, and $O_2^+(H_2O)_n$ depending on the position in the reaction region for three different reduced electric field strengths in the reaction region. In the model, a temperature of 45°C, a pressure of 14.3 mbar, and a background water concentration of 2000 ppm_v are assumed

converted into $H_3O^+(H_2O)_n$ while traversing the reaction region. This is in accordance with the simulated results in Figure 2 predicting the presence of only $H_3O^+(H_2O)_n$ ions at the end of the reaction region at x = 77 mm. However, according to the simulated results, in the vicinity of the corona discharge ionization source, considerable amounts of $NO^+(H_2O)_n$ and $O_2^+(H_2O)_n$ ions are still present in the reaction region. Furthermore, for example, at a reduced electric field strength in the reaction region of 115 Td, only small amounts of $O_2^+(H_2O)_n$ ions are observed in the recorded HiKE-IMS spectrum. However, at this reduced electric field strength, the conversion of $O_2^+(H_2O)_n$ into $H_3O^+(H_2O)_n$ proceeds rather slowly. Thus, inside the reaction region, significant amounts of $O_2^+(H_2O)_n$ are still present. It is important to note that ionization reactions in HiKE-IMS may occur anywhere in the reaction region. Therefore, to explain the origin of the product ion species observed in HiKE-IMS, the measured reactant ion spectra are of limited relevance, as they represent only the reactant ion population at the end of the reaction region.

4.2 | Formation of positive product ions from substances with low PA

Here, the occurring ionization pathways in HiKE-IMS are investigated based on the generated product ions of the four exemplary model substances: acetonitrile, methanol, phosphine, and benzene. Table 2 presents the thermochemical properties of these substances relevant

TABLE 2 Dipole moment (μ_D), polarizability (α), proton affinity (PA), and ionization energy (IE) of water, nitric oxide, and oxygen as well as the volatile organic compounds investigated in this work

Compound	Formula	Mass (u)	μ_D (D)	α (Å^3)	PA (kJ/mol)	IE (eV)
Water	H_2O	18	1.85	1.50	691	12.62
Nitric oxide	NO	30	0.15	1.70	532	9.26
Oxygen	O_2	32	0	1.56	421	12.07
Acetonitrile	C_2H_3N	41	3.92	4.28	779	12.2
Methanol	CH_3OH	32	1.7	3.28	754	10.84
Phosphine	PH_3	34	0.58	4.24	785	9.87
Benzene	C_6H_6	78	0	9.96	750	9.24

The stated values are taken from the NIST Chemistry WebBook[47] and the NIST Computational Chemistry Comparison and Benchmark DataBase.[60]

to ionization in HiKE-IMS. It is noteworthy that acetonitrile, methanol, phosphine, and benzene exhibit a low PA, ranging between that of H_2O (691 kJ/mol) and $(H_2O)_2$ (808 kJ/mol). Therefore, for all these substances, only PTRs with H_3O^+ are possible. However, acetonitrile, methanol, phosphine, and benzene differ in terms of their dipole moment and polarizability. Thus, regarding ligand-switching reactions, these substances should behave very differently in HiKE-IMS. Due to their similar high dipole moment and polarizability, acetonitrile and methanol should undergo efficient ligand-switching reactions with $H_3O^+(H_2O)_n$. In contrast, the nonpolar substances, phosphine and benzene, are hardly capable of undergoing ligand-switching reactions. Furthermore, acetonitrile, methanol, phosphine, and benzene have different IEs. Comparing the IE of NO with that of the stated substances, only benzene is thermodynamically capable of undergoing a charge-transfer reaction with NO^+. In addition, methanol, phosphine, and benzene exhibit a lower IE than O_2. Thus, a charge-transfer reaction between these substances and O_2 may be possible. However, the reaction of O_2^+ with methanol seems to be inefficient, proceeding significantly below the collisional rate.[26]

In this work, acetonitrile, methanol, phosphine, and benzene serve as model substances enabling a first evaluation of the capabilities and limitations of HiKE-IMS regarding the ionization of substances with low PA in positive ion mode.

The recorded positive HiKE-IMS spectra of acetonitrile, methanol, phosphine, and benzene are shown in Figure 3A for six different reduced electric field strengths in the reaction region. Again, the reduced electric field strength in the drift region is kept constant at 110 Td, the sample gas humidity is 4000 ppm_v, and the drift gas humidity is 50 ppm_v. To identify the product ion species underlying the peaks in the ion mobility spectrum, the product ion peaks marked in Figure 3A are transferred to the coupled mass spectrometer. In Figure 3B, the recorded mass spectra corresponding to the marked product ion peaks are shown.

In the HiKE-IMS spectrum of benzene, the benzene cation $C_6H_6^+$ (K_0 = 2.31 cm^2/Vs) and protonated benzene $C_6H_6H^+$ (K_0 = 2.24 cm^2/Vs) are observed. In the HiKE-IMS spectra of the other substances, only the protonated analyte molecules MH^+ occur. The reduced ion mobilities of the corresponding peaks are 2.66 cm^2/Vs ($C_2H_3NH^+$—protonated acetonitrile), 2.57 cm^2/Vs (CH_3OHH^+—protonated methanol), and 2.98 cm^2/Vs (PH_3H^+—protonated phosphine). It is noteworthy that a single charged phosphine PH_3^+ ion resulting from a charge-transfer reaction with O_2^+ does not occur in the HiKE-IMS spectra although this reaction is thermodynamically possible. However, we observe small m/z 34 signals underlying the peak of NO^+. Unfortunately, the peaks of NO^+ and PH_3^+ cannot be distinguished in the HiKE-IMS spectrum.

4.3 | Benzene cation $C_6H_6^+$

The benzene cation $C_6H_6^+$ may result from a charge-transfer reaction with either $NO^+(H_2O)_n$ or $O_2^+(H_2O)_n$. Thus, the relative abundances of the benzene cation $C_6H_6^+$ as a function of the reduced electric field strength in the reaction region provide information on the presence of $NO^+(H_2O)_n$ and $O_2^+(H_2O)_n$ ions in the reaction region in comparison with the measurable reactant ion population at the end of the reaction region. In Figure 4, the measured and simulated relative abundances of the benzene cation $C_6H_6^+$ are plotted against the reduced electric field strength in the reaction region. Three simulated relative abundances are shown: (a) only charge-transfer reactions with $NO^+(H_2O)_n$ are included in the model, (b) only charge-transfer reactions with $O_2^+(H_2O)_n$ are included in the model, and (c) charge-transfer reactions with both ions are included in the model. The simulated abundances are obtained from the kinetic model mentioned earlier assuming that a charge transfer to benzene occurs independently of the cluster size n at every collision with $NO^+(H_2O)_n$ and $O_2^+(H_2O)_n$, respectively. The corresponding collision rate constants are estimated from the permanent dipole moment and the polarizability of the analyte molecule applying the average-dipole-orientation theory with modified locking parameters, as presented in detail by Sekimoto et al.[61] The simulated abundances according to point (c) reach good agreement with the measured abundances, indicating that the benzene cation $C_6H_6^+$ results from charge-transfer reaction with both $NO^+(H_2O)_n$ and $O_2^+(H_2O)_n$.

Considering the measured relative abundance of the benzene cation $C_6H_6^+$ at the reduced electric field strength in the reaction region of 20 Td, it is noteworthy that small amounts of $C_6H_6^+$ ions are observed in the HiKE-IMS spectrum, although the reactant ion spectrum exhibits only the $H_3O^+(H_2O)_n$ signal. This result strongly indicates the presence of $NO^+(H_2O)_n$ and $O_2^+(H_2O)_n$ in the reaction region even at the reduced electric field strength of 20 Td. However, traversing the reaction region, $NO^+(H_2O)_n$ and $O_2^+(H_2O)_n$ are

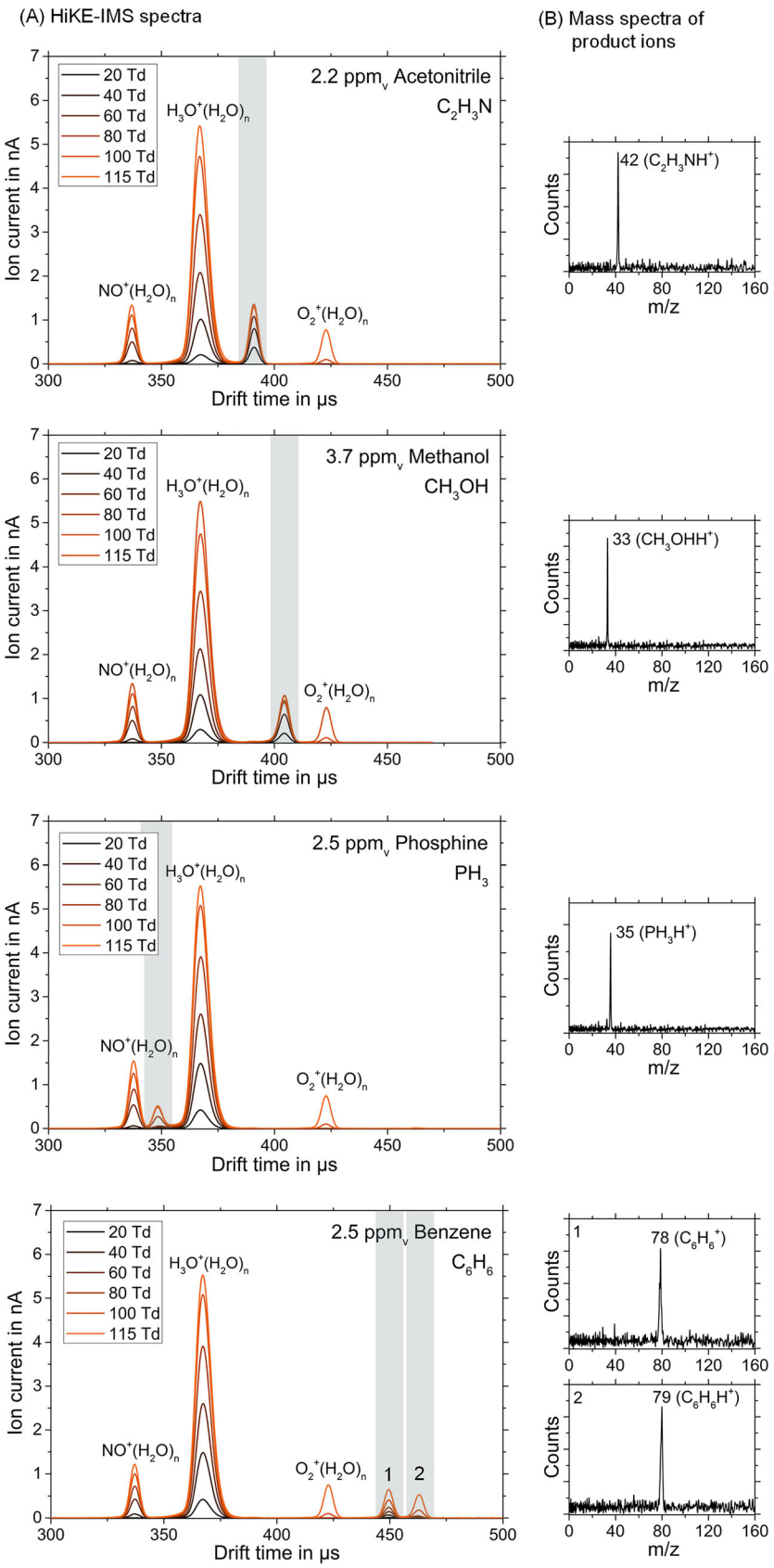

FIGURE 3 A, Positive high kinetic energy ion mobility spectrometry (HiKE-IMS) spectra of acetonitrile, methanol, phosphine, and benzene at different reduced electric field strengths in the reaction region and B, mass spectra corresponding to the marked product ion peaks in the HiKE-IMS spectra recorded by the HiKE-IMS-MS instrument operated in the selected-mobility mode. The sample gas humidity is 4000 ppm$_v$. The other operating parameters are provided in Table 1

converted into $H_3O^+(H_2O)_n$, and thus, neither $NO^+(H_2O)_n$ nor $O_2^+(H_2O)_n$ occurs in the spectrum. On increasing the reduced electric field strength in the reaction region up to 45 Td, the measured relative abundance of the $C_6H_6^+$ ions increases. In accordance with the simulated results, this is mainly due to an increasing presence of $NO^+(H_2O)_n$ in the reaction region. Furthermore, at reduced electric

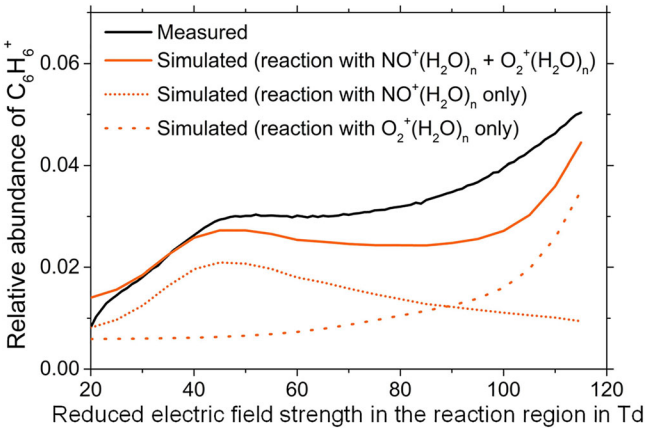

FIGURE 4 Measured and simulated relative abundances of the benzene cation $C_6H_6^+$ as a function of the reduced electric field strength in the reaction region. Three simulated curves are shown: (a) assuming that charge-transfer reactions with only $NO^+(H_2O)_n$ are possible, (b) assuming that charge-transfer reactions with only $O_2^+(H_2O)_n$ are possible, and (c) assuming that charge-transfer reactions with both ions are possible. The measured relative abundances are obtained from the measurements shown in Figure 3. The simulated abundances are obtained from the kinetic model described in a previous work,[22] assuming that a charge transfer to benzene occurs independently of the cluster size *n* at every collision with $NO^+(H_2O)_n$ and $O_2^+(H_2O)_n$, respectively

field strengths in the reaction region exceeding 70 Td, the measured relative abundance of the $C_6H_6^+$ ions increases further, as the conversion of $O_2^+(H_2O)_n$ into $H_3O^+(H_2O)_n$ is progressively inhibited and the amount of $O_2^+(H_2O)_n$ in the reaction region increases.

4.4 | Protonated analyte molecules

When considering the relative abundances of the protonated analyte molecules as a function of the reduced electric field strength in the reaction region, the proton transfer or ligand-switching reactions involving $H_3O^+(H_2O)_n$ can be analyzed in detail. In Figure 5A, the simulated proton-bound water cluster distribution at the end of the reaction region is shown. According to this water cluster distribution, the mean cluster size *n* of $H_3O^+(H_2O)_n$ in the reaction region decreases when the reduced electric field strength increases due to collision-induced cluster dissociation. At the reduced electric field strength of 20 Td, mainly $H_3O^+(H_2O)_4$ exists in the reaction region, whereas at reduced electric field strengths exceeding 110 Td, H_3O^+ is the most abundant ion species. As explained earlier, the presence of hydrated hydronium ions $H_3O^+(H_2O)_n$ in the reaction region at low reduced electric field strengths might significantly influence the formation of the protonated analyte molecule MH^+. However, as shown later, the magnitude of this effect strongly depends on the dipole moment and the polarizability of the respective analyte molecule.

In Figure 5B, the measured relative abundances of the protonated analyte molecules from acetonitrile, methanol, phosphine,

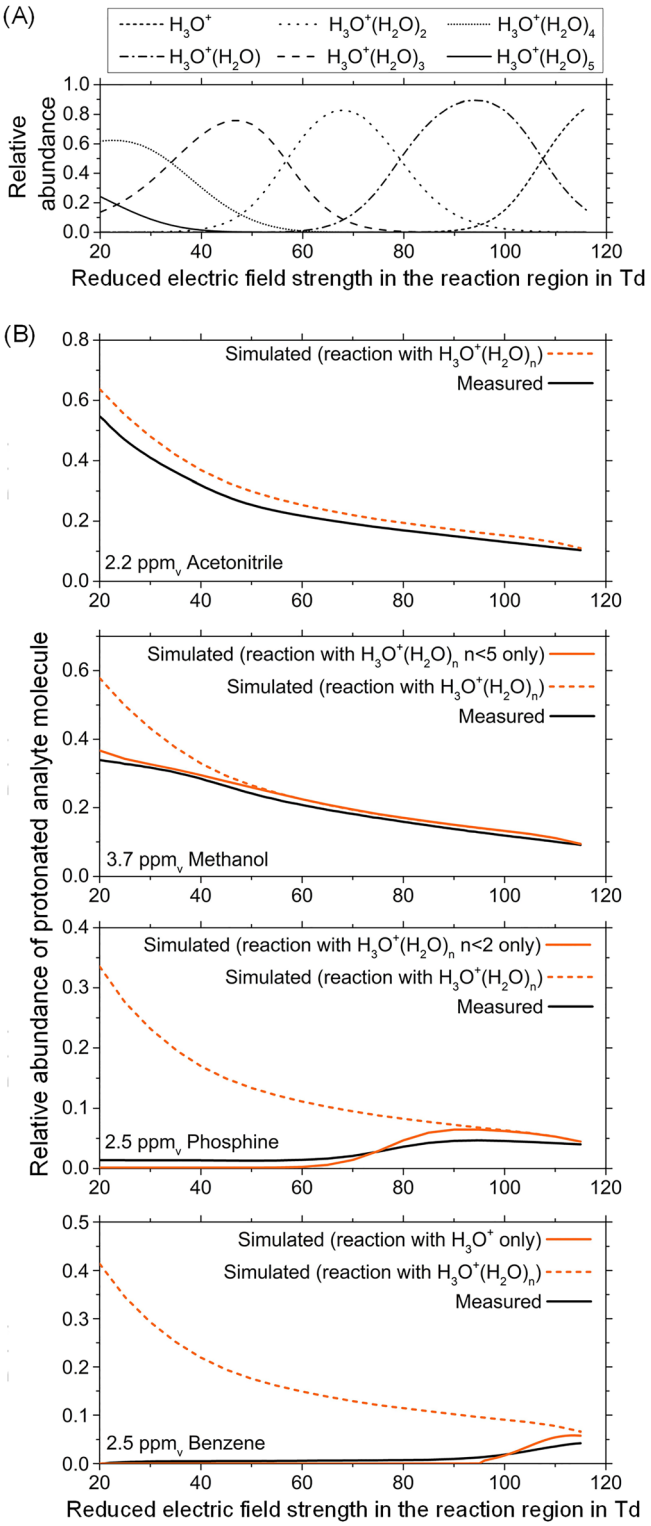

FIGURE 5 A, Simulated proton-bound water cluster distribution at the end of the reaction region of the HiKE-IMS instrument as a function of the reduced electric field strength in the reaction region. B, Measured and simulated relative abundances of the protonated analyte molecules of acetonitrile, methanol, phosphine, and benzene as a function of the reduced electric field strength in the reaction region. The measured relative abundances are obtained from the measurements shown in Figure 3. The simulated abundances are obtained from the kinetic model described in a previous work[22]

and benzene as a function of the reduced electric field strength in the reaction region are shown. In addition, Figure 5B shows simulated relative abundances, assuming that a reaction of the analyte molecule with $H_3O^+(H_2O)_n$ occurs independently of the cluster size n at every collision with $H_3O^+(H_2O)_n$ (dashed line). However, the assumption of a rate constant independent of the cluster size n is valid only for certain analyte molecules such as acetonitrile.

Acetonitrile exhibits a high permanent dipole moment of 3.92 D and a comparable high polarizability of 4.28 Å^3. Thus, acetonitrile should undergo efficient ligand-switching reactions with hydrated hydronium ions $H_3O^+(H_2O)_n$. Comparing the measured and simulated relative abundances of the protonated acetonitrile, the reaction of acetonitrile with $H_3O^+(H_2O)_n$ indeed seems to proceed almost independently of the cluster size n at every collision with $H_3O^+(H_2O)_n$.

In contrast, the measured relative abundances of the protonated methanol significantly deviate from the simulated relative abundances when assuming that the reaction of methanol with $H_3O^+(H_2O)_n$ occurs independently of the cluster size n at every collision. This deviation might be due to the lower permanent dipole of 1.7 D and the lower polarizability of 3.28 Å^3 of methanol causing the ligand-switching reactions between methanol and $H_3O^+(H_2O)_n$ to become more inefficient with increasing cluster size n.[18] For methanol, an agreement between measurement and simulation is reached when we assume that methanol reacts with $H_3O^+(H_2O)_n$ for $0 \le n \le 3$ independently of the cluster size n at every collision and with $H_3O^+(H_2O)_4$ only in 60% of all collisions.

The permanent dipole moment of phosphine (0.58 D) is even lower than that of methanol. Consequently, the deviation between the measured and simulated relative abundances when assuming that the reaction of phosphine with $H_3O^+(H_2O)_n$ occurs independently of the cluster size n at every collision is more pronounced. Reduced electric field strengths in the reaction region exceeding 70 Td are required to enable the generation of the protonated phosphine in HiKE-IMS. According to our measurements and simulations shown in Figure 5B, phosphine might thus undergo efficient ligand-switching reactions only with $H_3O^+(H_2O)$.

Finally, the protonated benzene is observed only at reduced electric field strengths in the reaction region exceeding 100 Td, indicating that the nonpolar molecule benzene does not react with any hydrated hydronium ion $H_3O^+(H_2O)_n$. This observation is in accordance with that from Ŝpaněl and Smith.[18]

In summary, these results confirm that the efficiency of ligand-switching reactions is significantly influenced by the dipole moment and the polarizability of the analyte molecule. In general, HiKE-IMS instruments should be operated at high reduced electric field strengths in the reaction region exceeding 110 Td. This is true for all analyte molecules for two reasons. First, as explained earlier, the total charge in the spectrum increases with the reduced electric field strength in the reaction region increasing the signal-to-noise ratio. Second, at these high reduced field strengths, the formation of large water clusters is inhibited due to collision-induced cluster dissociation, thus allowing for an efficient ionization of even nonpolar substances with low PA via PTRs with H_3O^+.

4.5 | Influence of humidity in the reaction region

When HiKE-IMS is used in field applications with a direct sample gas inlet, the sample gas humidity might range from 5% to 95% relative humidity (rH) at 298 K and 1013 mbar, leading to a relative humidity in the reaction region from 2.5% to 47%. Here, we state only the sample gas humidity, as this value is most relevant in the application. Due to the mixing ratio of the sample gas and the drift gas of 1:1, the conversion factor from sample gas humidity to reaction region humidity is 0.5. As stated earlier, to avoid the formation of large water clusters in the reaction region, the HiKE-IMS instrument should be operated at reduced electric field strengths in the reaction region exceeding 110 Td. On increasing the relative sample gas humidity from 5% to 95% at these high reduced electric field strengths, the prevailing reactant ion population present in the HiKE-IMS reaction region still changes. First, the amount of $O_2^+(H_2O)_n$ decreases, whereas the amount of $H_3O^+(H_2O)_n$ increases. Second, the average cluster size n of $H_3O^+(H_2O)_n$ shifts from 0 to 1.

As acetonitrile, methanol, and phosphine are capable of undergoing efficient reactions with both H_3O^+ and $H_3O^+(H_2O)$, the ionization of these substances is hardly affected when the relative sample gas humidity is varied. However, the effect of the sample gas humidity is more pronounced when considering the HiKE-IMS spectra of benzene. As shown in Figure 6, when the relative sample gas humidity is varied, the measured and the simulated relative abundances of the singly charged benzene $C_6H_6^+$ and the protonated benzene $C_6H_6H^+$ change. It is worth noting that the simulation agrees only qualitatively with the measurements. As shown in the previous work,[22] this is mainly due to a slightly incorrect modeling of the conversion from $O_2^+(H_2O)_n$ into $H_3O^+(H_2O)_n$ at elevated field strengths using the van't Hoff approach. Nonetheless, the simulation can be used to explain the measured curves. On increasing the sample gas humidity, the relative abundance of the benzene cation $C_6H_6^+$ in the spectra decreases. This is due to an increasing cluster association rate favoring the conversion of $O_2^+(H_2O)_n$ and $NO^+(H_2O)_n$ into protonated water clusters $H_3O^+(H_2O)_n$ inside the reaction region. Thus, the amount of $O_2^+(H_2O)_n$ and $NO^+(H_2O)_n$ available for ionizing benzene via charge transfer decreases. In contrast, between 4% and 12% relative sample gas humidity, the relative abundance of the protonated benzene $C_6H_6H^+$ ion increases. In this humidity range, the amount of H_3O^+ available for protonating benzene increases due to the conversion of $O_2^+(H_2O)_n$ into $H_3O^+(H_2O)_n$ followed by its collision-induced cluster dissociation. However, on increasing the relative sample gas humidity to values exceeding 12%, the relative abundance of the protonated benzene $C_6H_6H^+$ ion decreases again due to the increasing formation of hydrated hydronium ions $H_3O^+(H_2O)$ even at a high reduced field strength in the reaction region of 115 Td.

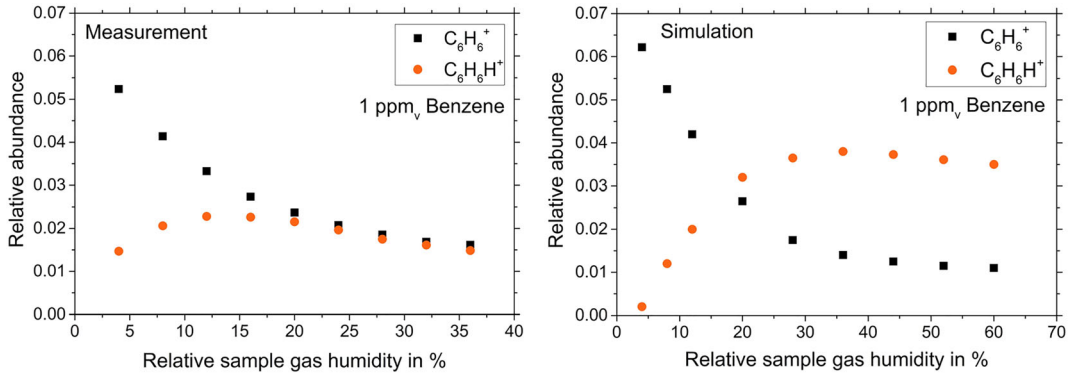

FIGURE 6 Measured and simulated relative abundances of the benzene cation $C_6H_6^+$ and the protonated benzene $C_6H_6H^+$ ion as a function of the relative sample gas humidity related to 298 K and 1013 mbar. The reduced electric field strength in the reaction region is 115 Td. The other operating parameters are provided in Table 1

4.6 | Capabilities and limitations of HiKE-IMS

The results presented demonstrate three fundamental aspects regarding analyte ionization that should be considered when using HiKE-IMS.

1. The reaction systems in HiKE-IMS are highly dynamic and may not reach chemical equilibrium at the end of the reaction region. This is especially true for the conversion of the initially generated $O_2^+(H_2O)_n$ and $NO^+(H_2O)_n$ ions into $H_3O^+(H_2O)_n$ that may take several hundreds of microseconds at 10–40 mbar depending on the reduced electric field strength and the background water concentration. This dynamic behavior makes a quantitative analysis difficult. However, compared with classical IMS the concept of HiKE-IMS significantly reduces chemical cross-sensitivities,[19] including the effect of water on peak height of analyte peaks.
2. The presence of the reactant ions $NO^+(H_2O)_n$ and $O_2^+(H_2O)_n$ may result in additional product ions that can be helpful in confirming the presence of analyte molecules and reducing the rate of false-positive responses. However, any distribution of charge among several product ions also impairs the limits of detection. The same applies for the reduced number of collisions between analyte molecules and reactant ions in HiKE-IMS.
3. In general, the HiKE-IMS instrument should be operated at high reduced electric field strengths in the reaction region exceeding 110 Td as the total charge in the spectrum increases with the reduced electric field strength in the reaction region. Furthermore, at these high reduced electric field strengths, the formation of ion–molecule clusters is largely inhibited in HiKE-IMS. Whereas hydrated hydronium ions $H_3O^+(H_2O)_n$ with $n \geq 3$ are the most abundant reactant ion species at ambient pressure,[48] bare or only slightly hydrated H_3O^+, NO^+, or O_2^+ ions are present in the HiKE-IMS instrument depending on the sample gas humidity. Thus, HiKE-IMS enables the ionization of, for example, substances with low PA that are not detected or are difficult to detect at ambient pressure. For example, the detection of benzene or phosphine with classical IMS is only possible using ambient pressure chemical ionization sources at low humidity levels[62-65] or using optical ionization sources.[66,67] In contrast, these analyte molecules can be easily observed in HiKE-IMS. Due to the inhibition of ion–molecule clusters at high reduced electric field strengths, HiKE-IMS enables the ionization of analyte molecules even when using sample gas containing water concentrations corresponding to high relative humidity between 5% and 95% at 25°C.

5 | CONCLUSIONS

In this work, the processes underlying the ionization of substances with low PA in HiKE-IMS were examined. The occurring ionization pathways were investigated based on the generated product ions of four exemplary substances: acetonitrile, methanol, phosphine, and benzene. Their product ions are identified using HiKE-IMS-MS. The substances exhibit a low PA ranging between those of H_2O and $(H_2O)_2$. Therefore, for all these substances, only PTRs with H_3O^+ are possible. However, acetonitrile, methanol, phosphine, and benzene differ in terms of their dipole moment, polarizability, and IE. Thus, they undergo different reactions in HiKE-IMS. Due to their similar high dipole moment and polarizability, acetonitrile and methanol undergo efficient ligand-switching reactions with $H_3O^+(H_2O)_n$. In contrast, the nonpolar substances phosphine and benzene are hardly capable of undergoing ligand-switching reactions. In addition to reactions with $H_3O^+(H_2O)_n$, the product ion population in HiKE-IMS may be affected by charge-transfer reactions with $NO^+(H_2O)_n$ and $O_2^+(H_2O)_n$. For example, benzene forms the cation $C_6H_6^+$ via charge-transfer reactions with these ions.

Comparing HiKE-IMS with classical IMS regarding trace gas detection, the assessment depends on the field of application. In general, the number of collisions between analyte molecules and reactant ions in HiKE-IMS is lower than in classical ambient pressure IMS. Considering the detection of polar substances with high PA, classical ambient pressure IMS thus reaches lower detection limits than HiKE-IMS. However, considering the detection of nonpolar

substances with low PA that are not detected or are difficult to detect at ambient pressure, HiKE-IMS would be beneficial. Furthermore, the much-shorter residence time of ions in the reaction region leads to a significant enhancement of the linear range and limited chemical cross-sensitivities in HiKE-IMS. Another important benefit of HiKE-IMS might be the possibility of changing the reduced electric field strength in the drift region independently of the reduced electric field in the reaction region to separate substances by their field-dependent ion mobility as known from field asymmetric ion mobility spectrometry and differential mobility spectrometry allowing for improved substance identification. Furthermore, high reduced electric field strengths can lead to fragmentation, also improving substance identification.

ACKNOWLEDGEMENTS

The authors thank Airsense Analytics for providing the chemicals used in this work. This work was funded by the Deutsche Forschungsgemeinschaft (DFG, German Research Foundation), joint project BE 2124/8-1–ZI 1288/8-1. Open access funding enabled and organized by Projekt DEAL.

PEER REVIEW

The peer review history for this article is available at https://publons.com/publon/10.1002/rcm.8998.

ORCID

Maria Allers https://orcid.org/0000-0001-8935-2739

REFERENCES

1. Puton J, Namieśnik J. Ion mobility spectrometry: Current status and application for chemical warfare agents detection. *Trends Anal Chem*. 2016;85:10-20.
2. Mäkinen MA, Anttalainen OA, Sillanpää MET. Ion mobility spectrometry and its applications in detection of chemical warfare agents. *Anal Chem*. 2010;82(23):9594-9600.
3. Mayer T, Borsdorf H. Which parameters influence the quantitative determination of halogenated substances? A summary of systematic investigations. *Int J Ion Mobil Spectrom*. 2015;18:33-39.
4. Gaik U, Sillanpää MET, Witkiewicz Z, Puton J. Nitrogen oxides as dopants for the detection of aromatic compounds with ion mobility spectrometry. *Anal Bioanal Chem*. 2017;409(12):3223-3231.
5. Zaknoun H, Binette M-J, Tam M. Analyzing fentanyl and fentanyl analogues by ion mobility spectrometry. *Int J Ion Mobil Spectrom*. 2019;22:1-10.
6. Armenta S, de la Guardia M, Alcalà M, Blanco M, Perez-Alfonso C, Galipienso N. Ion mobility spectrometry evaluation of cocaine occupational exposure in forensic laboratories. *Talanta*. 2014;130:251-258.
7. Ewing R. A critical review of ion mobility spectrometry for the detection of explosives and explosive related compounds. *Talanta*. 2001;54(3):515-529.
8. Mäkinen MA, Nousiainen M, Sillanpää MET. Ion spectrometric detection technologies for ultra-traces of explosives: A review. *Mass Spectrom Rev*. 2011;30(5):940-973.
9. Buryakov IA. Detection of explosives by ion mobility spectrometry. *J Anal Chem*. 2011;66:674-694.
10. Eiceman GA, Karpas Z, Hill HH. *Ion Mobility Spectrometry*. 3rd ed. Boca Raton, FL: CRC Press; 2014.
11. Borsdorf H, Mayer T, Zarejousheghani M, Eiceman GA. Recent developments in ion mobility spectrometry. *Appl Spectrosc Rev*. 2011;46:472-521.
12. Ross SK, Bell AJ. Reverse flow continuous corona discharge ionisation applied to ion mobility spectrometry. *Int J Mass Spectrom*. 2002;218:L1-L6.
13. Tabrizchi M, Khayamian T, Taj N. Design and optimization of a corona discharge ionization source for ion mobility spectrometry. *Rev Sci Instrum*. 2000;71:2321-2328.
14. Sabo M, Klas M, Wang H, Huang C, Chu Y, Matejčík Š. Positive corona discharge ion source with IMS/MS to detect impurities in high purity nitrogen. *Eur Phys J Appl Phys*. 2011;55:13808.
15. Sabo M, Matúška J, Matejčík Š. Specific O_2^- generation in corona discharge for ion mobility spectrometry. *Talanta*. 2011;85(1):400-405.
16. Ellis AM, Mayhew CA. *Proton Transfer Reaction Mass Spectrometry*. Chichester, UK: John Wiley & Sons, Ltd; 2014.
17. Bohme DK, Mackay GI, Tanner SD. An experimental study of the gas-phase kinetics of reactions with hydrated hydronium(1+) ions (n = 1-3) at 298 K. *J Am Chem Soc*. 1979;101:3724-3730.
18. Ŝpaněl P, Smith D. Reactions of hydrated hydronium ions and hydrated hydroxide ions with some hydrocarbons and oxygen-bearing organic molecules. *J Phys Chem*. 1995;99:15551-15556.
19. Langejuergen J, Allers M, Oermann J, Kirk AT, Zimmermann S. High kinetic energy ion mobility spectrometer: Quantitative analysis of gas mixtures with ion mobility spectrometry. *Anal Chem*. 2014;86:7023-7032.
20. Langejuergen J, Allers M, Oermann J, Kirk AT, Zimmermann S. Quantitative detection of benzene in toluene- and xylene-rich atmospheres using high-kinetic-energy ion mobility spectrometry (IMS). *Anal Chem*. 2014;86(23):11841-11846.
21. Allers M, Kirk AT, von Roßbitzky N, et al. Analyzing positive reactant ions in high kinetic energy ion mobility spectrometry (HiKE-IMS) by HiKE-IMS-MS. *J Am Soc Mass Spectrom*. 2020;31:812-821.
22. Allers M, Kirk AT, Eckermann M, et al. Positive reactant ion formation in high kinetic energy ion mobility spectrometry (HiKE-IMS). *J Am Soc Mass Spectrom*. 2020;31(6):1291-1301.
23. Allers M, Kirk AT, Timke B, et al. Negative reactant ion formation in high kinetic energy ion mobility spectrometry (HiKE-IMS). *J Am Soc Mass Spectrom*. 2020;31(9):1861-1874.
24. Kirk AT, Grube D, Kobelt T, Wendt C, Zimmermann S. High-resolution high kinetic energy ion mobility spectrometer based on a low-discrimination tristate ion shutter. *Anal Chem*. 2018;90(9):5603-5611.
25. Ŝpaněl P, Ji Y, Smith D. SIFT studies of the reactions of H3O+, NO+ and O2+ with a series of aldehydes and ketones. *Int J Mass Spectrom Ion Processes*. 1997;165-166:25-37.
26. Ŝpaněl P, Smith D. SIFT studies of the reactions of H3O+, NO+ and O2+ with a series of alcohols. *Int J Mass Spectrom Ion Process*. 1997;167-168:375-388.
27. Ŝpaněl P. Smith, D. SIFT studies of the reactions of H3O+, NO+ and O2+ with several ethers. *Int J Mass Spectrom Ion Process*. 1998;172:239-247.
28. Ŝpaněl P, Smith D. Selected ion flow tube studies of the reactions of H3O+, NO+, and O2+ with some organosulphur molecules. *Int J Mass Spectrom*. 1998;176:167-176.
29. Ŝpaněl P, Smith D. Selected ion flow tube studies of the reactions of H3O+, NO+, and O2+ with several aromatic and aliphatic hydrocarbons. *Int J Mass Spectrom*. 1998;181:1-10.
30. Ŝpaněl P, Smith D. Selected ion flow tube studies of the reactions of H3O+, NO+, and O2+ with several amines and some other nitrogen-containing molecules. *Int J Mass Spectrom*. 1998;176:203-211.
31. Ŝpaněl P, Smith D. SIFT studies of the reactions of H3O+, NO+ and O2+ with a series of volatile carboxylic acids and esters. *Int J Mass Spectrom Ion Process*. 1998;172:137-147.

32. Ŝpaněl P, Smith D. Selected ion flow tube studies of the reactions of H3O+, NO+, and O2+ with some chloroalkanes and chloroalkenes. *Int J Mass Spectrom*. 1999;184:175-181.
33. Ŝpaněl P, Smith D. Selected ion flow tube studies of the reactions of H3O+, NO+, and O2+ with several aromatic and aliphatic monosubstituted halocarbons. *Int J Mass Spectrom*. 1999;189:213-223.
34. Ŝpaněl P, Smith D. Selected ion flow tube studies of the reactions of H3O+, NO+, and O2+ with eleven amine structural isomers of c5h13n. *Int J Mass Spectrom*. 1999;185-187:139-147.
35. Wang T, Smith D, Ŝpaněl P. Selected ion flow tube studies of the reactions of H3O+, NO+ and O2+ with the anaesthetic gases halothane, isoflurane and sevoflurane. *Rapid Commun Mass Spectrom*. 2002;16:1860-1870.
36. Ŝpaněl P, Wang T. Smith, D. a selected ion flow tube, SIFT, study of the reactions of H3O+, NO+ and O2+ ions with a series of diols. *Int J Mass Spectrom*. 2002;218:227-236.
37. Diskin AM, Wang T, Smith D, Ŝpaněl P. A selected ion flow tube (SIFT), study of the reactions of H3O+, NO+ and O2+ ions with a series of alkenes; in support of SIFT-MS. *Int J Mass Spectrom*. 2002; 218:87-101.
38. Wang T, Ŝpaněl P, Smith D. Selected ion flow tube, SIFT, studies of the reactions of H3O+, NO+ and O2+ with eleven C10H16 monoterpenes. *Int J Mass Spectrom*. 2003;228:117-126.
39. Ŝpaněl P, Diskin AM, Wang T. Smith, D. a SIFT study of the reactions of H3O+, NO+ and O2+ with hydrogen peroxide and peroxyacetic acid. *Int J Mass Spectrom*. 2003;228:269-283.
40. Malásková M, Olivenza-León D, Piel F, et al. Compendium of the reactions of H3O+ with selected ketones of relevance to breath analysis using proton transfer reaction mass spectrometry. *Front Chem*. 2019;7:401.
41. Brown P, Watts P, Märk TD, Mayhew CA. Proton transfer reaction mass spectrometry investigations on the effects of reduced electric field and reagent ion internal energy on product ion branching ratios for a series of saturated alcohols. *Int J Mass Spectrom*. 2010;294: 103-111.
42. Mochalski P, Unterkofler K, Španěl P, Smith D, Amann A. Product ion distributions for the reactions of NO+ with some physiologically significant aldehydes obtained using a SRI-TOF-MS instrument. *Int J Mass Spectrom*. 2014;363:23-31.
43. Jordan A, Haidacher S, Hanel G, et al. An online ultra-high sensitivity proton-transfer-reaction mass-spectrometer combined with switchable reagent ion capability (PTR+SRI−MS). *Int J Mass Spectrom*. 2009;286:32-38.
44. Atkins PW, de Paula J, Keeler J. *Atkins' Physical Chemistry*. Oxford, New York: Oxford University Press; 2018.
45. Smith D, Ŝpaněl P. Ambient analysis of trace compounds in gaseous media by SIFT-MS. *Analyst*. 2011;136:2009-2032.
46. Su T, Bowers MT. Ion-polar molecule collisions: The effect of ion size on ion-polar molecule rate constants; the parameterization of the average-dipole-orientation theory. *Int J Mass Spectrom Ion Process*. 1973;12:347-356.
47. Linstrom P, Mallard WG. *NIST Chemistry WebBook, NIST Standard Reference Database 69*; 2020.
48. Wissdorf W, Seifert L, Derpmann V, Klee S, Vautz W, Benter T. Monte Carlo simulation of ion trajectories of reacting chemical systems: Mobility of small water clusters in ion mobility spectrometry. *J Am Soc Mass Spectrom*. 2013;24(4):632-641.
49. Cheng H-P. Water clusters: Fascinating hydrogen-bonding networks, solvation shell structures, and proton motion. *J Phys Chem a*. 1998; 102:6201-6204.
50. Wròblewski T, Ziemczonek L, Karwasz GP. Proton transfer reactions for ionized water clusters. *Czechoslov J Phys*. 2004;54:C747-C752.
51. Goebbert DJ, Wentold PG. Water dimer proton affinity from the kinetic method: Dissociation energy of the water dimer. *Eur J Mass Spectrom*. 2004;10:837-846.
52. Raksit AB, Bohme DK. An experimental study of the influence of hydration on the reactivity of the hydroxide anion in the gas phase at room temperature. *Can J Chem*. 1983;61:1683-1689.
53. Bohme DK, Mackay GI. Bridging the gap between the gas phase and solution: Transition in the kinetics of nucleophilic displacement reactions. *J Am Chem Soc*. 1981;103:978-979.
54. Takashima K, Riveros JM. Gas-phase solvated negative ions. *Mass Spectrom Rev*. 1998;17:409-430.
55. Borsdorf H, Fiedler P, Mayer T. The effect of humidity on gas sensing with ion mobility spectrometry. *Sens Actuators B*. 2015;218:184-190.
56. de Gouw J, Warneke C, Karl T, Eerdekens G, van der Veen C, Fall R. Sensitivity and specificity of atmospheric trace gas detection by proton-transfer-reaction mass spectrometry. *Int J Mass Spectrom*. 2003;223–224:365-382.
57. Smith D, Wang T, Ŝpaněl P. A SIFT study of the reactions of H2ONO + ions with several types of organic molecules. *Int J Mass Spectrom*. 2003;230:1-9.
58. Kirk AT, Kobelt T, Spehlbrink H, Zimmermann S. A simple analytical model for predicting the detectable ion current in ion mobility spectrometry using corona discharge ionization sources. *J Am Soc Mass Spectrom*. 2018;29(7):1425-1430.
59. Wannier GH. Motion of gaseous ions in strong electric fields. *Bell Syst Tech J*. 1953;32:170-254.
60. Johnson RD. *Computational Chemistry Comparison and Benchmark Database, NIST Standard Reference Database 101*. National Institute of Standards and Technology; 2019.
61. Sekimoto K, Li S-M, Yuan B, et al. Calculation of the sensitivity of proton-transfer-reaction mass spectrometry (PTR-MS) for organic trace gases using molecular properties. *Int J Mass Spectrom*. 2017; 421:71-94.
62. Borsdorf H, Schelhorn H, Flachowsky J, Döring H-R, Stach J. Corona discharge ion mobility spectrometry of aliphatic and aromatic hydrocarbons. *Anal Chim Acta*. 2000;403:235-242.
63. Kim SH, Betty KR, Karasek FW. Plasma chromatography of benzene with mass identified mobility spectra. *Anal Chem*. 1978;50:1784-1788.
64. Zimmermann S, Gunzer F. Simultaneous detection of benzene and toluene using a pulsed ion mobility spectrometer. *Sens Actuators B*. 2013;188:106-110.
65. Sabo M, Matejčík Š. Corona discharge ion mobility spectrometry with orthogonal acceleration time of flight mass spectrometry for monitoring of volatile organic compounds. *Anal Chem*. 2012;84(12): 5327-5334.
66. Baumbach JI, Sielemann S, Xie Z, Schmidt H. Detection of the gasoline components methyl tert-butyl ether, benzene, toluene, and m-xylene using ion mobility spectrometers with a radioactive and UV ionization source. *Anal Chem*. 2003;75(6):1483-1490.
67. Sielemann S, Baumbach JI, Schmidt H, Pilzecker P. Quantitative analysis of benzene, toluene, and m-xylene with the use of a UV-ion mobility spectrometer. *Field Analyt Chem Technol*. 2000;4:157-169.

SUPPORTING INFORMATION

Additional supporting information may be found online in the Supporting Information section at the end of this article.

How to cite this article: Allers M, Kirk AT, Schaefer C, Schlottmann F, Zimmermann S. Formation of positive product ions from substances with low proton affinity in high kinetic energy ion mobility spectrometry. *Rapid Commun Mass Spectrom*. 2021;35:e8998. https://doi.org/10.1002/rcm.8998